



HAL
open science

Deposition of metallic silver coatings by Aerosol Assisted MOCVD using two new silver [small beta]-diketonate adduct metalorganic precursors

Hongjun Liu, S. Battiato, A. L. L Pellegrino, P. Paoli, P. Rossi, Carmen Jimenez, G. Malandrino, David Muñoz-Rojas

► To cite this version:

Hongjun Liu, S. Battiato, A. L. L Pellegrino, P. Paoli, P. Rossi, et al.. Deposition of metallic silver coatings by Aerosol Assisted MOCVD using two new silver [small beta]-diketonate adduct metalorganic precursors. Dalton Transactions, 2017, 46 (33), pp.10986-10995. 10.1039/C7DT01647F . hal-01758856

HAL Id: hal-01758856

<https://hal.science/hal-01758856>

Submitted on 13 Nov 2018

HAL is a multi-disciplinary open access archive for the deposit and dissemination of scientific research documents, whether they are published or not. The documents may come from teaching and research institutions in France or abroad, or from public or private research centers.

L'archive ouverte pluridisciplinaire **HAL**, est destinée au dépôt et à la diffusion de documents scientifiques de niveau recherche, publiés ou non, émanant des établissements d'enseignement et de recherche français ou étrangers, des laboratoires publics ou privés.

Deposition of metallic silver coatings by Aerosol Assisted MOCVD using two new silver β -Diketonate adduct metalorganic precursors

Received 00th January 20xx,
Accepted 00th January 20xx

DOI: 10.1039/x0xx00000x

www.rsc.org/

H. Liu^a, S. Battiato^b, A. L. Pellegrino^b, P. Paoli^c, P. Rossi^c, C. Jiménez^a, G. Malandrino^b and D. Muñoz-Rojas^{a,*}

Abstract: This work reports two new silver metalorganic precursors for the chemical vapor deposition of Ag metallic coatings. Both precursors are based on β -diketonate adducts, namely, Ag(hfac)(L) (H-hfac= 1,1,1,5,5,5-hexafluoro-2,4-pentanedione), where L is 1,10-phenanthroline (phen) or 2,5,8,11-tetraoxadodecane (triglyme). Using these ligands, the designed precursors have better solubility in alcoholic solvents and are less toxic and costly than previously reported ones. The new precursors have been characterized and their crystallographic structure solved. With the new triglyme precursor, [Ag(triglyme)₂]⁺[Ag(hfac)₂]⁻, pure metallic Ag coatings made of Ag nanoparticles about 20 nm in diameter were successfully deposited on glass and Si substrates using Aerosol Assisted Metalorganic CVD (AA-CVD).

Introduction

Silver is a noble metal with unique physical properties including high conductivity and plasmonic, anti-bacterial and self-cleaning effects.^{1–3} Metalorganic Chemical Vapor Deposition (MOCVD) is an industrially relevant technique for obtaining functional coatings, including Ag metallic coatings. In MOCVD, the process can be largely altered by the way in which precursors are designed and delivered. Thus, depending on how precursors are fed into the deposition chamber, MOCVD is classified into several branches: Hot Wall CVD (HW-CVD), Cold Wall CVD (CW-CVD), Pulsed Injection CVD (PI-CVD), Aerosol Assisted CVD (AA-CVD), etc.⁴

This big family of MOCVD systems also brings new challenges for the design of new silver precursors. In particular, AA-CVD is an interesting CVD approach since it operates at ambient pressure. For AA-CVD, alcohol solvents are preferred due to the concerns related to the use of other more hazardous solvents, thus precursors being soluble in alcohol solvents are desirable.^{5,6} In the case of the currently known silver metalorganic precursors, solubility in alcohols is low since silver complex molecules tend to polymerise when dissolved in the solvent. This limits the number of available silver precursors suitable for AA-CVD systems. AgNO₃ has indeed been reported as precursor for Ag coatings using AA-MOCVD by N. Bahlawane *et al.* and Ponja *et al.*^{7,8} But given the non-organometallic nature

Table 1. Reported silver metal organic precursors used in metalorganic CVD.

Metalorganic Precursor	CVD variant	Solvents	Deposition Temperature / °C	Ref
(hfac)Ag(BTMSA)	HW-CVD	none	~ 250	⁹
(hfac)Ag(SEt ₂)	AA-CVD	Toluene	n.a.	¹⁰
[Ag(O ₂ CC ₃ F ₇)(PPh ₃) ₂]	AA-CVD	THF	310	¹¹
Ag(fod)(PEt ₃)	PI-CVD	None (Liquid precursor)	220	¹²
(hfac)Ag(VTES)	CW-CVD	None (Liquid precursor)	220	¹³
(tfac)AgP(OEt) ₃	CW-CVD	None (Liquid precursor)	180	¹⁴
(C ₂ F ₅ COO)Ag(PMe ₃)	HW-CVD	n.a.	200	¹⁵
Ag(hfac)(PPh ₃)	AA-CVD	THF	310	¹⁶
Ag(O ₂ CtBu)(PMe ₃)	HW-CVD	n.a.	180	¹⁷
Silver carboxylates	PI-CVD	Mesitylene	300	¹⁸

Notes: **H-hfac**: 1,1,1,5,5,5-hexafluoro-2,4-pentanedione; **H-tfac**: 1,1,1-trifluoro-2,4-pentanedione; **Hfod**: 6,6,7,7,8,8,8-heptafluoro-2,2-dimethyl-3,5-octanedione **BTMSA**: bis(trimethylsilyl)acetylene; **SEt₂**: Ethyl sulphide; **VTES**: vinyltriethylsilane; **PEt₃**: triethylphosphine; **P(OEt)₃**: triethylphosphite; **PMe₃**: Trimethylphosphine; **PPh₃**: Triphenylphosphine; **O₂CtBu**: 2,2,6,6-tetramethyl-3,5-heptanedionate

of AgNO₃, the utilization of such precursor may be limited to some type of CVD reactors. In addition, the development of new organometallic Ag precursors is also interesting, for instance for application in ALD, where suitable Ag precursors

^a Univ. Grenoble Alpes, CNRS, Grenoble INP, LMGP, F-38000 Grenoble, France.

^b Dipartimento di Scienze Chimiche, Università Degli Studi di Catania, INSTM Udr-Catania, Catania, Italy.

^c Dipartimento di Ingegneria Industriale, Università Degli Studi di Firenze, Italy.

† Footnotes relating to the title and/or authors should appear here.

See DOI: 10.1039/x0xx00000x

are still needed, especially for thermal ALD¹⁹). As shown in **Table 1**, the different silver metalorganic precursors reported to date were mostly used in conventional or PI-CVD systems. Few examples of ALD of Ag coatings have also been reported previously.^{20–25} In the cases where AA-CVD was used, non-environmentally friendly solvents, such as THF and toluene, were used in combination with organometallic precursors.^{10,11,16} Concerning the design of Ag metalorganic precursors, previous works have introduced different systems, including β -diketonate adducts $\text{Ag}(\text{hfac})(\text{L})$ ²⁶ or $\text{Ag}(\text{fod})(\text{L})$, where L were tertiary phosphines (PPh_3), 2,5,8,11,14-pentaoxapentadecane or bis(trimethylsilyl)-acetylene) or carboxylates ($\text{Ag}(\text{O}_2\text{C-L})$).^{9,11,15} Apart from the low solubility of these precursors in alcohol solvents, other issues such as low volatility or the high toxicity of the ligands have been also reported.^{14, 16, 20} In addition, some of the ligands are rather expensive, contributing to a higher price of the final Ag precursor. Thus, new silver precursors with less toxic ligands, good solubility in alcohol solvents and clean rapid decomposition, are still needed, ideally using less expensive ligands.

In this work, two new silver metalorganic precursors with general formula $\text{Ag}(\text{hfac})\text{-L}$ were designed and synthesized using different ligands: $[\text{Ag}(\text{hfac})(\text{phen})]$ (**AgP**, phen=1,10-phenanthroline) and $[\text{Ag}(\text{triglyme})_2]^+[\text{Ag}(\text{hfac})_2]^-$ (**AgT**, triglyme = 2,5,8,11-tetraoxadodecane). In addition, all the ligands Hfac, triglyme and phenanthroline are not very expensive, thus reducing the final precursor cost. In this study we describe the synthesis and characterization of these new silver complexes and the results of their use as precursors for the deposition of Ag coatings via AA-CVD with alcohol solvents.

Experimental

Starting materials: Ag_2O (99%, Strem Chemicals), H-hfac (99%, Strem Chemicals), triglyme (99%, Sigma Aldrich), 1,10-phenanthroline (anhydrous 99%, Strem Chemicals), dichloromethane (99.8%, Sigma Aldrich), and n-pentane (99%, Sigma Aldrich) were used as received for the synthesis.

Synthesis of $[\text{Ag}(\text{hfac})(\text{phen})]$ (AgP**):** The synthesis was performed suspending 2.20 g of Ag_2O (9.49 mmol) in 50 ml of dichloromethane. 2.54 g of Phenanthroline (14.14 mmol) were then added to the suspension. After 10 min, 2.94 g of H-hfac (14.14 mmol) were added to the mixture, which was refluxed under stirring for 1 h. Excess silver oxide was filtered off. Lastly, yellow crystals were obtained after removal of the solvent upon evaporation. A pure crystalline solid was obtained after purification with small quantities of n-pentane, in which the adduct is insoluble, and then vacuum dried. The reaction yield was 72%. The melting point of the crude product was 158–164 °C (dec.) (760 Torr). Elemental analysis for **AgP** ($\text{C}_{17}\text{H}_9\text{AgF}_6\text{N}_2\text{O}_2$): Calc: C, 41.23; H, 1.83; N, 5.66. Found: C, 41.35; H, 1.71; N, 5.78.

Synthesis of $[\text{Ag}(\text{triglyme})_2]^+[\text{Ag}(\text{hfac})_2]^-$ (AgT**):** The synthesis was conducted following a similar procedure to that used for **AgP** from Ag_2O (2.20 g, 9.49 mmol), triglyme (2.528 g, 14.14 mmol) and H-hfac (2.94 g, 14.14 mmol). Pure light yellow

crystals were obtained after purification with n-pentane. The reaction yield was 82%. The melting point of the crude product was 62–65 °C (760 Torr). Elemental analysis for **AgT**

Table 2. Single crystal crystallographic data and refinement parameters for AgP and

	AgP	AgT
<i>Chemical formula</i>	$[\text{Ag}(\text{hfa})(\text{phen})]$	$[\text{Ag}(\text{triglyme})_2]^+ [\text{Ag}(\text{hfa})_2]^-$
<i>Empirical formula</i>	$\text{C}_{17}\text{H}_9\text{AgF}_6\text{N}_2\text{O}_2$	$\text{C}_{26}\text{H}_{38}\text{Ag}_2\text{F}_{12}\text{O}_{12}$
<i>Formula weight</i>	495.13	986.30
<i>Temperature (K)</i>	100	250
<i>Wavelength (Å)</i>	1.54184	0.71073
<i>Crystal system, space group</i>	Triclinic, P-1	Triclinic, P-1
<i>Unit cell dimensions (Å, °)</i>	$a = 7.4309(3)$ $b = 9.2288(4)$ $c = 13.1426(6)$ $\alpha = 102.579(4)$ $\beta = 105.172(4)$ $\gamma = 103.608(4)$	$a = 11.4965(6)$ $b = 12.9561(7)$ $c = 13.0344(9)$ $\alpha = 96.821(5)$ $\beta = 91.795(5)$ $\gamma = 92.350(4)$
<i>Volume (Å³)</i>	807.10(6)	1924.8(2)
<i>Z, D_c (mg/cm³)</i>	2, 2.037	2, 1.702
<i>μ (mm⁻¹)</i>	10.823	1.127
<i>F(000)</i>	484	984
<i>Crystal size (mm)</i>	0.30x0.27x0.20	0.28x0.25x0.19
<i>θ range (°)</i>	5.165 to 72.336	4.111 to 29.400
<i>Reflections collected / unique</i>	8748 / 3045	13020 / 7438
<i>Data / parameters</i>	3045 / 295	7438 / 519
<i>Goodness-of-fit on F²</i>	1.115	1.061
<i>Final R indices [$I > 2\sigma(I)$]</i>	R1 = 0.0407, wR2 = 0.0934	R1 = 0.0637, wR2 = 0.1714
<i>R indices (all data)</i>	R1 = 0.0565, wR2 = 0.1169	R1 = 0.0876, wR2 = 0.1942

AgT.

($\text{C}_{26}\text{H}_{38}\text{Ag}_2\text{F}_{12}\text{O}_{12}$): Calc: C, 31.66; H, 3.88. Found: C, 31.52; H, 3.76.

XRD analyses and structure elucidation: The molecular and crystal structures of **AgP** and **AgT** were studied by means of single crystal X-ray diffraction. Measurements were carried out with an Oxford Diffraction Excalibur diffractometer using the Cu-K α radiation ($\lambda = 1.54184$ Å) for **AgP** and Mo-K α radiation ($\lambda = 0.71073$ Å) for **AgT**. Data collection and data reductions were performed with the program CrysAlis Pro. Finally, absorption correction was performed with the program ABSPACK.²⁷ Structures were solved by using the SIR-2004 package²⁸ and subsequently refined on the F_2 values by the full-matrix least-squares program SHELXL-2013.²⁹ Geometrical calculations were performed by PARST97³⁰ and molecular plots were produced by the program Mercury (v3.7).³¹ The crystal data and refinement parameters of the new Ag adducts are reported in **Table 2**. Single crystals of **AgT** were twinned. Two domains were taken into account during

refinement. The fluorine atoms bound to the carbon atom C5 of the -hfac anion, in **AgP** are disordered. Such disorder was modelled by introducing three positions for each fluorine atom (refined occupancy factors: 0.44, 0.41, 0.15). In **AgT** all the CF₃ moieties are disordered. Such a disorder was modelled by introducing two positions for each fluorine atom bonded to C4, C5 and C10 (refined occupancy factors: 0.62/0.38 for the atoms bonded to C4; 0.83/0.17 for the atoms bonded to C5; 0.76/0.34 for the atoms bonded to C10) In addition all the atoms of C4(F₃) moiety were set in double position (refined occupancy factors: 0.55/0.45). For all the non-hydrogen atoms in **AgP** and **AgT**, anisotropic thermal parameters were used. For the hydrogen atoms in **AgP**, they were found in the Fourier difference map and their positions were freely refined, while their thermal parameters were refined accordingly to the bound atoms. The hydrogen atoms in **AgT** were introduced in calculated position and refined in agreement with the carbon atom to which they are bound.

Characterization of Ag precursors: Elemental microanalysis were performed using a Carlo Erba 1106 elemental analyser. Fourier Transform Infrared Spectroscopy (FT-IR) was done using a Jasco FT/IR-430 spectrometer with nujol mulls between NaCl plates. ¹H NMR (400.13 MHz) and ¹³C NMR (100.61 MHz) were acquired on a Bruker Avance™ 400 spectrometer. Chemical shifts (δ) are expressed in parts per million (ppm). Spectra were referenced to the residual proton solvent peaks; coupling constant (J) values are given in Hz. Thermogravimetric analyses were made using a Mettler Toledo TGA/SDTA 851e. Dynamic thermal analyses were carried out under purified nitrogen flow (30 sccm) at atmospheric pressure with a 5 °C/min heating rate. Weights of the samples were between 10-15 mg. Melting points were taken on very small single crystals using a Kofler hot-stage microscope.

Deposition parameters: The depositions of Ag coatings were conducted in a home-made AA-CVD system at 320 °C, using ethanol as solvent with a concentration of 0.01 M. 2 L/min and 5 L/min of N₂ were used as carrier gas and accelerating gas, respectively. The solution consumption rate was fixed at around 1.4 ml/min and deposition duration was between 30 to 90 min, glass (Corning Glass) and Si wafers were used as substrate. The detailed parameters are shown in **Table 3**.

Characterization of the Ag coatings: the Ag coatings were analysed using a Scanning Electron Microscope (SEM-FEG Environmental FEI QUANTA 250). Particle diameter distribution was calculated from SEM images using the Image J software.³² The Ag coating were scratched for further characterization with Transmission Electron Microscopy (TEM-JEM2010-JEOL). Carbon residues were analysed with RAMAN Spectroscopy (Jobin Yvon/Horiba LabRam) equipped with a liquid nitrogen cooled charge coupled device detector.

Table 3. Deposition parameters of Ag coatings in Aerosol CVD

Sample names	Precursor used	Deposition Duration (h)
P1	[Ag(hfac)(phen)]	0.5
P2	(AgP)	1.5

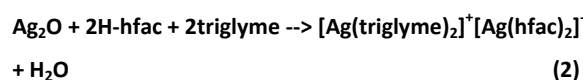
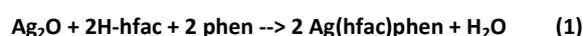
T1	[Ag(triglyme) ₂]	0.5
T2	[Ag(hfac) ₂] ⁻ (AgT)	1.5

A 488 nm wavelength Ar⁺ ion laser beam was used with 300 s acquisition duration by 2 cycles. Grazing Incidence (0.35°) X-Ray Diffraction (GI-XRD, Bruker D8) was performed using Cu Kα radiation (40 kV, 40 mA), with 2θ angle ranging from 30° to 80° with a step size 0.06° and acquisition time 33 s/step.

Results and discussion

Precursor synthesis, structure and properties

The synthesis of **AgP** and **AgT** adducts was carried out through a single step reaction, from silver (I) oxide, hexafluoroacetylacetonate and the neutral ligands, phenanthroline or triglyme, in dichloromethane, as described above and shown in **Equations (1)** and **(2)**.



In both cases, the synthesis was reproducible and yielded an anhydrous product. Adducts were soluble in dichloromethane and could be isolated as yellow crystalline powders by removal of the solvent. The silver precursors were characterized by FT-IR spectroscopy in the wave number range of 4000-500 cm⁻¹. The results for **AgP** and **AgT** are shown in **Fig. 1 a)** and **b)** respectively. In both cases, the FT-IR spectra do not show bands in the 3300–3600 cm⁻¹ interval, which indicates the absence of water coordinated to the silver cation. Peaks at 2923, 1461, and 1375 cm⁻¹ are associated with the nujol used to prepare the mull. In both silver complexes, the β-diketonate

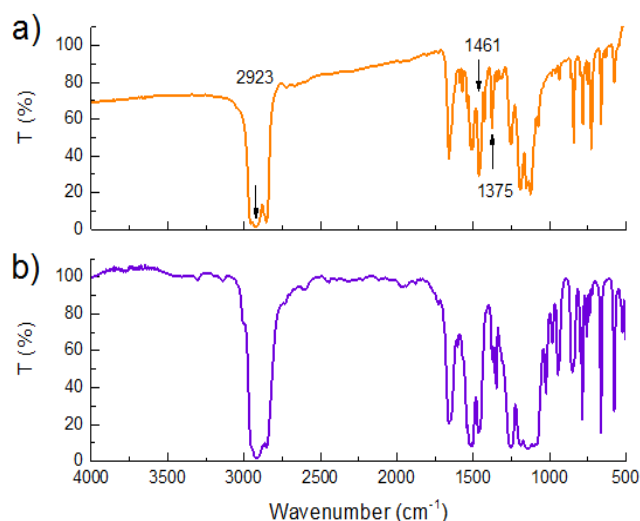
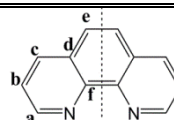


Figure 1. FT-IR spectra of **AgP** (a) and **AgT** (b) in nujol.

Table 4. ^1H and ^{13}C NMR of AgP and AgT.

complex	^1H NMR		^{13}C NMR			
	-CO-CH-CO	Phen*	-CO-CH-CO	-CO-CH-CO	-CF ₃	Phen*
AgP	5.79 (s, 1H)	a 9.04 (s, 2H), b 7.79 (m, 2H), c 8.40 (dd, 2H) e 7.89 (d, 2H)	86.38 (s)	176.91 (q, $^2J=32\text{Hz}$)	117.63 (q, $^1J=288\text{ Hz}$)	a 150.99, b , 124.40, c 137.81, d 128.94, e 126.89, f 142.13
complex	^1H NMR		^{13}C NMR			
	-CO-CH-CO	polyether [†]	-CO-CH-CO	-CO-CH-CO	-CF ₃	polyether [†]
AgT	5.81 (s, 1H)	a 3.60 (s, 6H), b, c 3.62 (m, 8H), d 3.71 (s, 4H)	86.12 (s)	176.84 (q, $^2J=32\text{Hz}$)	117.56 (q, $^1J=289\text{ Hz}$)	a 61.21, b, c 70.11, 70.58, d 71.42

*The following notation has been used for phenanthroline.



[†]The following notation has been used for triglyme. $(\text{CH}_3\text{-O-CH}_2\text{-CH}_2\text{-O-CH}_2)_2$.

a
b
c
d

while the C=C stretching vibration is associated with the absorptions at 1500-1550 cm^{-1} . In addition, the bands present in the interval 1050-1400 cm^{-1} can be attributed to typical C-F vibrations of the -hfa ligand present in both adducts. For **AgP**, the bands observed in the 700–1100 cm^{-1} range are considered fingerprints of the phenanthroline coordination to silver ion. In **AgT**, the broad band observed in the 1000-1300 cm^{-1} range might be associated with absorptions from polyether C-O bending and/or stretching overlapped with the C-F stretching of the β -diketonate. Furthermore, bands at 700-1100 cm^{-1} are related with glyme modes. The C-H glyme stretching modes, lying in the 2800-3000 cm^{-1} range, overlap with nujol features. ^1H and ^{13}C NMR of AgP and AgT were recorded in CDCl_3 (Table 4). The ^1H NMR spectrum of AgP (Fig. S1) has been attributed in accordance to the assignments of references ^{33,34}. The

spectrum shows a singlet (5.79 δ) associated with the ring proton of the hfa ligand, while the phenanthroline shows peaks in the typical range of aromatic ligand from 7.6 to 9.1 δ . The **a** protons are observed as a singlet at 9.04 δ , the **b** proton as a multiplet at 7.79 δ , the **c** protons as a doublet of doublets at 8.40 δ and, finally, the **e** protons as a doublet at 7.89 δ . The phen peaks have been assigned following the notation reported as a note in table 4. The 1:1 (hfa:phen) ratio (Fig. S1) found through evaluation of intensities of pertinent resonances finds counterpart in the ratio obtained through single crystal X-ray diffraction. The ^{13}C NMR spectrum of AgP (Fig. S2) shows resonances associated with the coordinated hfa ligand, which consist of a singlet ($\delta \approx 86$) for the CH group, quartets ($\delta \approx 118$) for the CF_3 groups and quartets ($\delta \approx 177$) for the CO groups. The quartets are due to first order (CF_3 ; $^1J = 288$

AgP		Bond Angles (°)	
		N(1)-Ag-N(2)	71.4(2)
Bond distances (Å)		O(1)-Ag-O(2)	79.4(1)
Ag-N(1)	2.369(6)	N(1)-Ag-O(1)	165.4(2)
Ag-N(2)	2.327(4)	N(2)-Ag-O(2)	158.8(1)
Ag-O(1)	2.276(5)	N(1)-Ag-O(2)	87.6(2)
Ag-O(2)	2.439(3)	N(2)-Ag-O(1)	121.1(2)
AgT		Bond Angles (°)	
Bond Distance (Å)		O(5)-Ag(1)-O(10)	76.0(2)
Ag(1)-O(1)	2.329(5)	O(5)-Ag(1)-O(11)	95.5(2)
Ag(1)-O(2)	2.275(5)	O(5)-Ag(1)-O(12)	85.7(2)
Ag(1)-O(3)	2.340(5)	O(6)-Ag(1)-O(7)	64.0(2)
Ag(1)-O(4)	2.261(4)	O(6)-Ag(1)-O(8)	125.1(2)
Ag(2)-O(5)	2.662(6)	O(6)-Ag(1)-O(9)	82.8(2)
Ag(2)-O(6)	2.626(8)	O(6)-Ag(1)-O(10)	130.0(2)
Ag(2)-O(7)	2.618(7)	O(6)-Ag(1)-O(11)	145.5(2)
Ag(2)-O(8)	2.792(7)	O(6)-Ag(1)-O(12)	84.8(3)
Ag(2)-O(9)	2.550(6)	O(7)-Ag(1)-O(8)	62.7(2)
Ag(2)-O(10)	2.661(7)	O(7)-Ag(1)-O(9)	81.0(2)
Ag(2)-O(11)	2.568(8)	O(7)-Ag(1)-O(10)	138.4(2)
Ag(2)-O(12)	2.559(8)	O(7)-Ag(1)-O(11)	133.7(2)
Bond Angles (°)		O(7)-Ag(1)-O(12)	96.8(2)
O(1)-Ag(1)-O(2)	79.8(2)	O(8)-Ag(1)-O(9)	100.9(2)
O(1)-Ag(1)-O(3)	111.1(2)	O(8)-Ag(1)-O(10)	99.1(2)
O(1)-Ag(1)-O(4)	127.3(2)	O(8)-Ag(1)-O(11)	74.0(2)
O(2)-Ag(1)-O(3)	125.6(2)	O(8)-Ag(1)-O(12)	89.1(1)
O(2)-Ag(1)-O(4)	135.7(2)	O(9)-Ag(1)-O(10)	65.4(2)
O(3)-Ag(1)-O(4)	81.0(2)	O(9)-Ag(1)-O(11)	124.9(2)
O(5)-Ag(1)-O(6)	63.6(2)	O(9)-Ag(1)-O(12)	167.1(3)
O(5)-Ag(1)-O(7)	127.0(2)	O(10)-Ag(1)-O(11)	61.7(2)
O(5)-Ag(1)-O(8)	169.5(2)	O(10)-Ag(1)-O(12)	121.3(2)
O(5)-Ag(1)-O(9)	85.6(2)	O(11)-Ag(1)-O(12)	65.5(3)

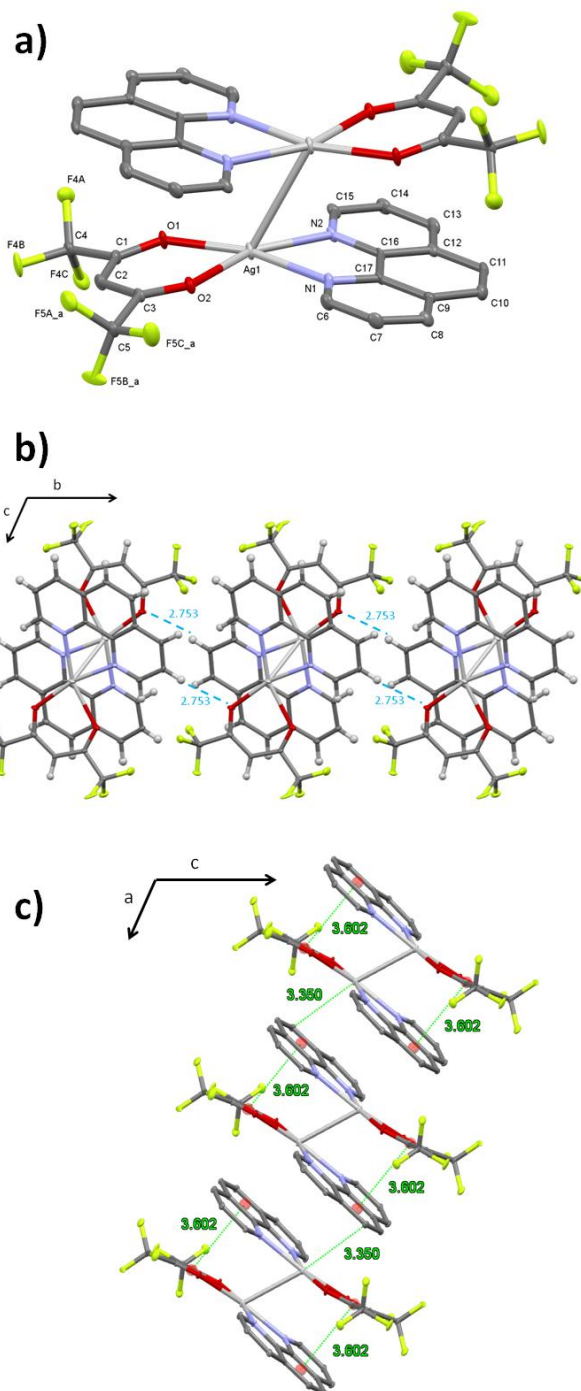
Hz) and second order (CO; $^2J = 32$ Hz) coupling with the CF_3 fluorine atoms. The coordinated phenanthroline signals are observed in the range of 127-152 δ . Assignments are reported in the table 4 together with the notation used for phenanthroline.

The 1H NMR spectrum of AgT (Table 4) can be assigned using comparative arguments with data from the related lanthanum complex.³¹ The spectrum (Fig. S3) shows a singlet at 5.81 δ associated with the ring proton of the hfa ligand. Different resonances are associated with the triglyme framework. The methyl groups (**a** protons) are always observed as a singlet at $\delta = 3.60$. The **b** and **c** protons are observed as a multiplet centered at $\delta = 3.62$. The protons **d** are associated with a singlet at $\delta = 3.71$. Evaluation of intensities of pertinent resonances points to a 1:1 (hfa: triglyme) ratio in accordance with single crystal X-ray diffraction.

The ^{13}C NMR spectrum of AgT (Fig. S4) is similar to that found for the AgP adduct in regard to the hfa ligand. Resonances associated with the coordinated hfa ligand consist of a singlet ($\delta \approx 86$) for the CH group, a quartet ($\delta \approx 117$) for the CF_3 groups and a quartet ($\delta \approx 177$) for the CO groups. The quartets are due

to Hz;
triç
OC
Tab

The
sin
of
y,
bo
an
slig
be:
dis
atç
ge
Bo
thi
fo
dis
Ag



same reason just one model of the disordered CF₃ moiety was shown). b) along the *b* axis direction showing the intra- and inter-dimer π -stacking interactions. Hydrogen atoms were omitted (top); c) along the *a* axis direction showing the CH...O intermolecular interactions. For the sake of clarity just one model of the -hfac fluorine atoms bound to C5.

Figure 2. structure c

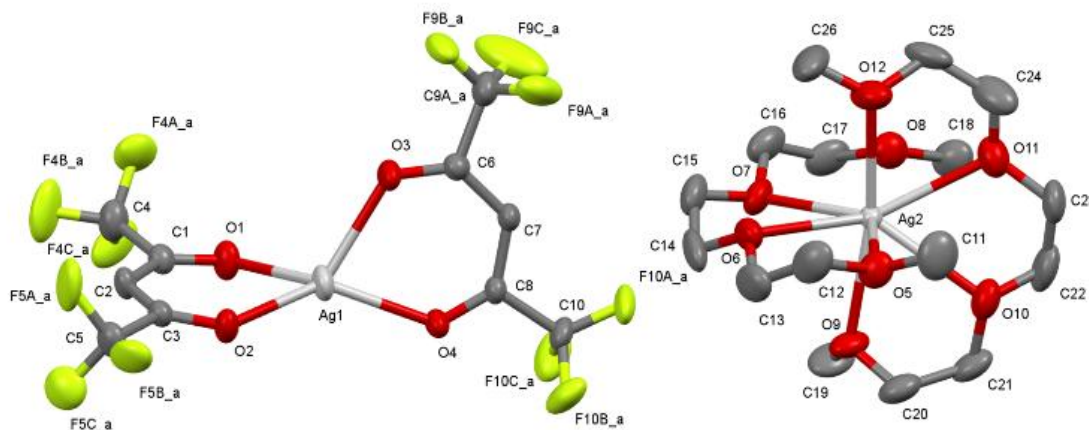


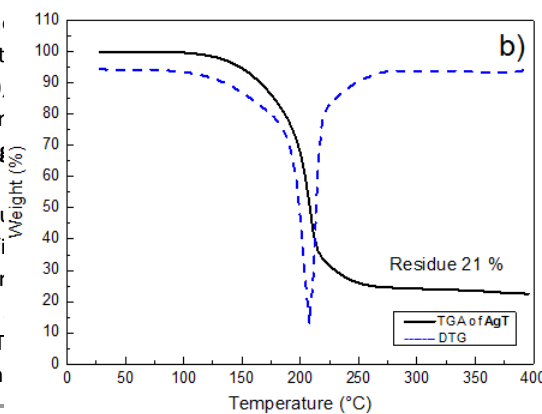
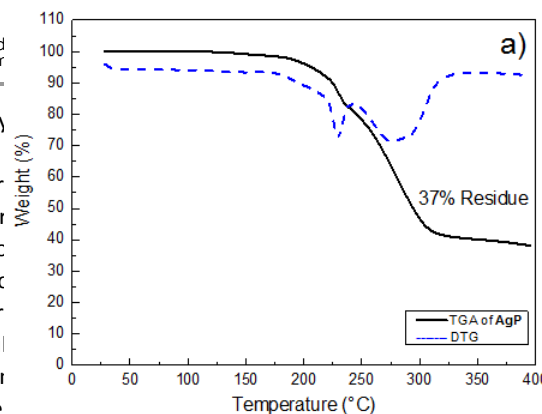
Figure 3. View of the [Ag(triglyme)₂]⁺ cation and [Ag(hfac)₂]⁻ anion in AgT (ellipsoids are drawn at the 50% probability level. Hydrogen atoms were omitted for clarity. For the sake of clarity just one model of the -hfac fluorine atoms (which were disordered and refined isotropically) is shown. For the sake of clarity just one model of the -hfac fluorine atoms bound to C5.

3.60(1)Å and the angle between the C_T-C_T line and the mean phen plane is 71.2(2)°. Centroid of the hfa ring as defined by O(1)C(2)C(1)C(3)O(2), centroid of the central ring of phen as defined by C(9)C(10)C(11)C(12)C(16)C(17)).

Finally, the dimers stack along the *a* axis in a head-to-tail arrangement (Fig. 2 b), which brings the carbon atom C(10) of a symmetry related (-x, -y, 2-z) phen molecule 3.350(8) Å apart from the silver ion, with a distance less than the sum of the Van der Waals radii (3.81 Å)⁴¹. In addition, inter-dimer π stacking interactions involving the phen molecules provided by two contiguous dimers are present (the mean phen planes are 3.5 Å apart). Finally, dimers propagate along the *b* axis (Fig. 2 c) through a weak C(7)H(7)...O(1)' intermolecular interaction (*l*' = x, 1+y, z; D...A and H...A distances 3.628(6) and 2.75(6) Å, respectively, DHA angle 161(6)°).

The solid state structure of compound AgT was also determined by means of single crystal X-ray diffraction. In the asymmetric unit of AgT one [Ag(triglyme)₂]⁺ cation and one [Ag(hfac)₂]⁻ anion are present (Fig. 3). In the two ions, the silver atom shows different coordination spheres. In fact, in the [Ag(triglyme)₂]⁺ cation, the silver atom Ag(2) is surrounded by two triglyme molecules and bound to all the eight oxygen atoms that those ligands provide. It is worth noting that, although one Ag-O distance [i.e. Ag(1)-O(8)] is longer than the others (see Table 5), it is inside the Ag-O range as retrieved in the Cambridge Structural Database (CSD v. 5.37).⁴¹ The two

triglyme molecules are coordinated to the silver atom in a bidentate fashion. The coordination of the silver atom is completed by the two hfac ligands. The silver atom is also coordinated to the oxygen atoms of the hfac ligands. The silver atom is also coordinated to the oxygen atoms of the hfac ligands. The silver atom is also coordinated to the oxygen atoms of the hfac ligands.



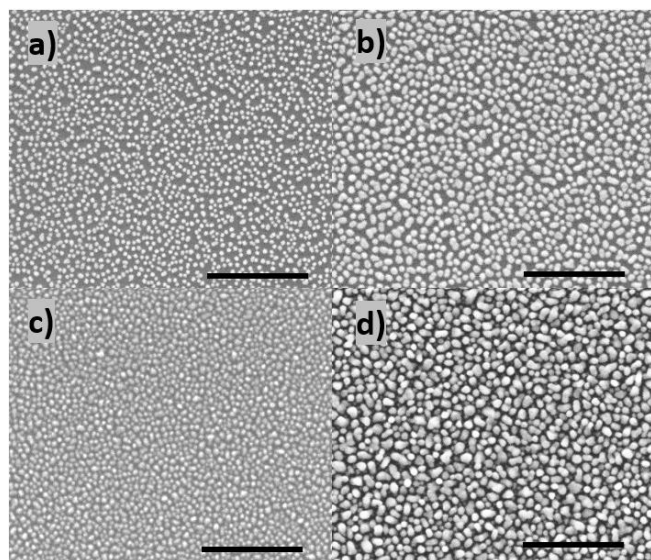


Figure 4. Thermogravimetric Analysis (TGA) and its derivative curves (DTG) of precursors, between 30 °C and 400 °C, of a) AgP and b) AgT.

Thus it can be concluded that the precursor does not present a clean decomposition, with some organic species still remaining at 400 °C. Conversely, the TGA curve related to **AgT** (Fig. 4 b) shows a single (see derivative) rapid weight loss in the range 150-250 °C, yielding a 22.5% residue when heating to 400 °C. The stoichiometric Ag weight portion in the precursor being 21.9%, the value obtained from TGA is thus well tuned with the expected percentage of metallic silver in the compound, implying a clean and complete decomposition of the precursor. By comparing the TGA results for those two precursors, **AgT** appears as a better silver metalorganic precursor.

Silver coatings by MOCVD and characterizations

To test the two silver precursors, depositions at 320 °C for different durations were carried out in a homemade Aerosol Assisted CVD system, as detailed above in Table 3. Both precursors were carefully grinded before being dissolved in ethanol, reaching 10 mM concentration at room temperature. Comparing the results of depositions using the different precursors, **AgT** showed higher deposition efficiency than **AgP** (see SEM images in Fig. 5). For a deposition duration of 0.5 h, **AgP** yielded a yellow coating while **AgT** gave an orange colour with a higher particle density (Fig. 5 a) and c)). Increasing the deposition duration to 1.5 h, coatings from **AgP** and **AgT** both presented purple colour coatings but the grain density for the latter was still higher than for the former (Fig. 5 b) and d)). For the deposition conditions used, the particles in the coating are not connected and thus the samples present high resistance

values, namely a sheet resistance of $5 \times 10^8 \Omega/\text{cm}^2$ measured by 4 probes. As well, the adhesion between the Ag coating and glass substrate is poor and the films can be easily removed.

Figure 5. Scanning Electron Microscopy images of silver coatings deposited at 320 °C by AA-CVD using: AgP precursor with deposition duration a) 0.5 h (P1); b) 1.5 hrs (P2); and AgT precursor with deposition duration c) 0.5 h (T1); d) 1.5 hrs (T2). Scale bars in figures are 500 nm.

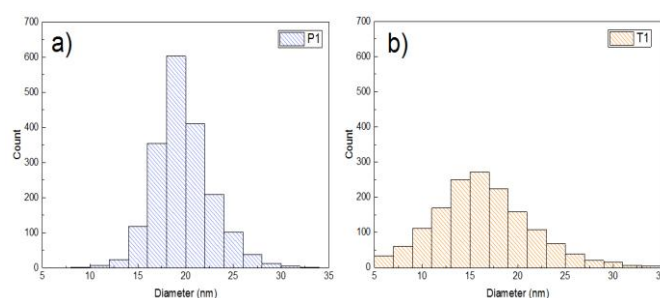


Figure 6. Size distribution of Ag nanoparticles deposited from: P1 (a) and T1 (b).

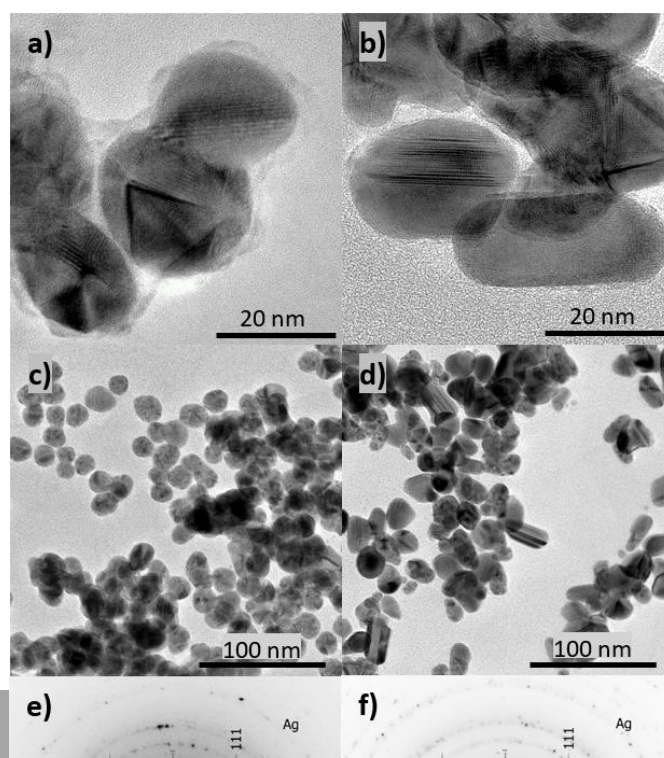


Figure 7. Transmission Electron Microscopy images and electron diffractions for Ag particles deposited using **AgP** (**P2**, a, c, e) and **AgT** (**T2**, b, d, f).

By analysing the different particle diameters, a narrower size distribution of Ag grains from **P1** is revealed from comparing **Fig. 6 a)** and **b)**. The size of grains from **P1** is mainly located around 19 nm, while particles obtained from **T1** range broadly distributed from 10 nm to 22 nm. Such a different size distribution can be related to the thin carbon layer.

As shown in **Fig. 7 a)** and **b)**, the coatings obtained with both precursors present well crystallized Ag nanoparticles, but from the sample deposited with **AgP** (**P2**), a thin shell surrounding the Ag nanoparticles was observed. Also, as already hinted by TEM images (**Fig. 7 c)** and **d)**), Ag nanoparticles obtained from **AgP**

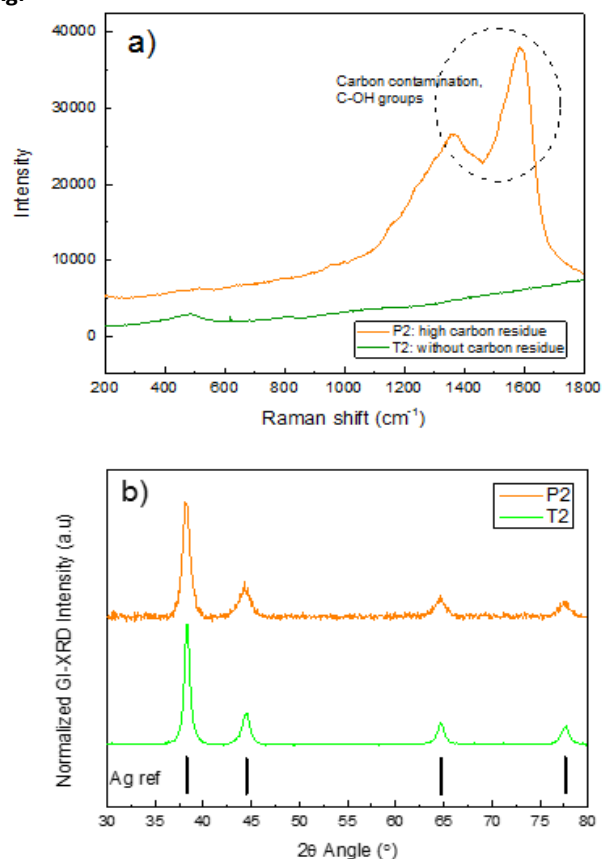


Figure 8. Characterization of silver coatings deposited with the different precursors. a) RAMAN spectroscopy for carbon residues detection; b) Normalized GI-XRD patterns of silver coatings deposited on glass substrate.

gave more regular round shapes than those obtained from **AgT** (**T2**), which are elongated. Electron diffraction patterns of the different particles show diffraction rings which only correspond to metallic Ag. To further evaluate the purity and crystallinity of the coatings obtained from the two precursors, Raman spectroscopy and X-Ray Diffraction were used and the results are shown in **Fig. 8**. **Fig. 8 a)** shows the Raman spectrum obtained for silver particles deposited using **AgP**.

In this case, strong peaks related to the C-OH group in the range 1200 cm^{-1} and 1600 cm^{-1} can be observed, in agreement with the presence of the carbonaceous shell observed by TEM.

On the other hand, coatings deposited with **AgT** showed a flat band curve in this high wavenumber range. XRD patterns of the two different coatings are shown in **Fig. 8 b)**. Comparing the XRD pattern of silver coatings from **AgT** (green curve) and from **AgP** (orange curve), in both cases the XRD patterns show the characteristic reflections of the face centered cubic Ag phase, confirming the formation of crystalline Ag coatings, and the smaller crystallite size for coatings deposited with **AgP**.

The carbon contaminations found for AgP, both by Raman and TEM, are due to the incomplete decomposition of the precursor under the deposition conditions used, and are in agreement with the TGA results shown above. Thus, although AgP is able to yield Ag coatings when used as precursor in AA-CVD, these present carbon species which are expected to affect the properties of the final coating (i.e. conductivity) and thus can be not suitable for certain applications.

Conclusions

In this work, two new silver metal organic precursors have been synthesized using less expensive and toxic ligands, namely, $[\text{Ag}(\text{hfac})\text{phen}]$ (**AgP**) and $[\text{Ag}(\text{triglyme})_2]^+[\text{Ag}(\text{hfac})_2]^-$ (**AgT**). FTIR spectroscopy has confirmed the formation of such molecular complexes. Furthermore, the crystal structures of both precursors were solved by means of single crystal X-ray diffraction. TGA analyses have shown that **AgT** is a precursor with a more rapid and clean decomposition than **AgP**. The new adducts present enough solubility in ethanol and have been tested in an Aerosol Assisted CVD system. Depositions by AA-CVD revealed that the two precursors, used under similar CVD parameters, produced coatings with different surface morphologies. Coatings deposited from AgP are made of Ag nanoparticles presenting a carbonaceous shell. Conversely, Ag coatings from **AgT** consist of pure Ag nanoparticles and present high crystallinity. In conclusion, our results show that the new **AgT** adduct is a good precursor for depositing metallic Ag coatings via AA-CVD using alcohol solvents.

Acknowledgements

HL acknowledges the Ministère de l'Éducation nationale, de l'Enseignement supérieur et de la Recherche in France for a Ph.D. grant. DMR acknowledges funding through the Marie

Curie Actions (FP7/2007- 2013, Grant Agreement No. 631111). The authors thank the University Italo-Francese for financial support through the Galileo 2014-2015 program (G14-148). CRIST (Centro di Cristallografia Strutturale, Università degli Studi di Firenze, Italy) where single-crystal X-ray data were collected is also thanked. O. Chaix is thanked for her assistance with Raman characterization. L. Rapenne is thanked for performing TEM characterization. Dr. C. Geraci from the Institute of Biomolecular Chemistry, National Research Council (C.N.R.), Catania, Italy is thanked for performing the NMR spectra.

References

- 1 C.-Y. Cho, M.-K. Kwon, S.-J. Lee, S.-H. Han, J.-W. Kang, S.-E. Kang, D.-Y. Lee and S.-J. Park, *Nanotechnology*, 2010, **21**, 205201.
- 2 J. H. Hsieh, C. H. Chiu, C. Li, W. Wu and S. Y. Chang, *Surf. Coatings Technol.*, 2013, **233**, 159–168.
- 3 N. A. Janunts, K. S. Baghdasaryan, K. V. Nerkararyan and B. Hecht, *Opt. Commun.*, 2005, **253**, 118–124.
- 4 J. Melorose, R. Perroy and S. Careas, *Chemical Vapor Deposition Book*, Springer Science+Business media, LLC, 2015, vol. 1.
- 5 P. Marchand, I. A. Hassan, I. P. Parkin and C. J. Carmalt, *Dalton Trans.*, 2013, **42**, 9406–22.
- 6 C. E. Knapp and C. J. Carmalt, *Chem. Soc. Rev.*, 2016, **45**, 1036–1064.
- 7 S. D. Ponja, S. K. Sehmi, E. Allan, A. J. MacRobert, I. P. Parkin and C. J. Carmalt, 2015, 3–10.
- 8 N. Bahlawane, P. A. Premkumar, A. Brechling, G. Reiss and K. Kohse-Höinghaus, *Chem. Vap. Depos.*, 2007, **13**, 401–407.
- 9 B. K. Chi and Y. Lu, *Chem. Vap. Depos.*, 2001, **7**, 117–120.
- 10 C. Xu, M. J. Hampden-smith, T. T. Kostas, E. N. Dueslert, A. L. Rheingold and G. Yap, *Inorg. Chem.*, 1995, **34**, 4767–4773.
- 11 D. A. Edwards, R. M. Harker, M. F. Mahon and K. C. Molloy, *Inorganica Chim. Acta*, 2002, **328**, 134–146.
- 12 L. Gao, P. Härter, C. Linsmeier, J. Gstöttner, R. Emling and D. Schmitt-Landsiedel, *Mater. Sci. Semicond. Process.*, 2004, **7**, 331–335.
- 13 L. Gao, P. Härter, C. Linsmeier, a. Wiltner, R. Emling and D. Schmitt-Landsiedel, *Microelectron. Eng.*, 2005, **82**, 296–300.
- 14 H.-K. Kim, H.-C. Jeong, K. S. Kim, S. H. Yoon, S. S. Lee, K. W. Seo and I.-W. Shim, *Thin Solid Films*, 2005, **478**, 72–76.
- 15 E. Szłyk, P. Piszczek, A. Grodzicki, M. Chaberski, A. Goliński, J. Szatkowski and T. Błaszczuk, *Chem. Vap. Depos.*, 2001, **7**, 111–116.
- 16 D. A. Edwards, M. F. Mahon, K. C. Molloy and V. Ogrodnik, *J. Mater. Chem.*, 2003, **13**, 563–570.
- 17 P. Piszczek, E. Szłyk, M. Chaberski, C. Taeschner, A. Leonhardt, W. Bała and K. Bartkiewicz, *Chem. Vap. Depos.*, 2005, **11**, 53–59.
- 18 M. Abourida, H. Guillon, C. Jiménez, J. M. Decams, F. Weiss, O. Valet and P. Doppel, *Electrochem. Soc.*, 2003, **Proceeding**, 938–945.
- 19 M. Ritala, M. Leskela, J. Hämäläinen, M. Ritala and M. Leskelä, *Chem. Mater.*, 2013, **26**, 786–801.
- 20 H. K. Kim, H. C. Jeong, K. S. Kim, S. H. Yoon, S. S. Lee, K. W. Seo and I. W. Shim, *Thin Solid Films*, 2005, **478**, 72–76.
- 21 L. Zanotto, F. Benetollo, M. Natali, G. Rossetto, P. Zanella, S. Kaciulis and A. Mezzi, *Chem. Vap. Depos.*, 2004, **10**, 207–213.
- 22 A. Niskanen, T. Hatanpää, K. Arstila, M. Leskelä and M. Ritala, *Chem. Vap. Depos.*, 2007, **13**, 408–413.
- 23 M. Kariniemi, J. Niinistö, T. Hatanpää, M. Kemell, T. Sajavaara, M. Ritala and M. Leskelä, *Chem. Mater.*, 2011, **23**, 2901–2907.
- 24 Y. C. Liang, C. C. Wang, C. C. Kei, Y. C. Hsueh, W. H. Cho and T. P. Perng, *J. Phys. Chem. C*, 2011, **115**, 9498–9502.
- 25 V. A. Sivakov, K. Höflich, M. Becker, A. Berger, T. Stelzner, K. E. Elers, V. Pore, M. Ritala and S. H. Christiansen, *ChemPhysChem*, 2010, **11**, 1995–2000.
- 26 M. E. Fragalà, G. Malandrino, O. Puglisi and C. Benelli, *Chem. Mater.*, 2000, **12**, 290–293.
- 27 L. Massai, D. Cirri, E. Michelucci, G. Bartoli, A. Guerri, M. A. Cinellu, F. Cocco, C. Gabbiani and L. Messori, *BioMetals*, 2016, **29**, 863–872.
- 28 M. C. Burla, R. Caliendo, M. Camalli, B. Carrozzini, G. L. Cascarano, L. De Caro, C. Giacovazzo, G. Polidori and R. Spagna, *J. Appl. Crystallogr.*, 2005, **38**, 381–388.
- 29 G. M. Sheldrick, *Acta Crystallogr. Sect. C Struct. Chem.*, 2015, **71**, 3–8.
- 30 M. Nardelli, *J. Appl. Crystallogr.*, 1995, **28**, 659.
- 31 C. F. Macrae, I. J. Bruno, J. A. Chisholm, P. R. Edgington, P. McCabe, E. Pidcock, L. Rodriguez-Monge, R. Taylor, J. van de Streek and P. A. Wood, *J. Appl. Crystallogr.*, 2008, **41**, 466–470.
- 32 A. G. Young and L. R. Hanton, *Coord. Chem. Rev.*, 2008, **252**, 1346–1386.
- 33 R. H. and C. D. M. Frechette, I. R. Butler, *Inorg. Chem.*, 1992, **31**, 1650–1656.
- 34 L. Thornton, V. Dixit, L. O. N. Assad, T. P. Ribeiro, D. D. Queiroz, A. Kellett, A. Casey, J. Colleran, M. D. Pereira, G. Rochford, M. McCann, D. O’Shea, R. Dempsey, S. McClean, A. F.-A. Kia, M. Walsh, B. Creaven, O. Howe and M. Devereux, *J. Inorg. Biochem.*, 2016, **159**, 120–132.
- 35 G. Malandrino, C. Benelli, F. Castelli, I. L. Fragala, S. Chimiche and V. A. Doria, 1998, 3434–3444.
- 36 F. H. Allen, *Acta Crystallogr. Sect. B*, 2002, **58**, 380–388.
- 37 F. Pointillart, P. Herson, K. Boubekeur and C. Train, *Inorganica Chim. Acta*, 2008, **361**, 373–379.
- 38 1962 International Tables for X-ray Crystallography, Kynoch Press, Birmingham, vol. 3, .
- 39 P. W. Griffith, T. Y. KOH, A. J. P. White and D. J. Williams, *Polyhedron*, 1995, **14**, 2019–2025.
- 40 N. Venkatalakshmi and M. V. Rajasekharan, *Transit. Met. Chem*, 1992, **17**, 455–457.
- 41 Edited by W. M. Haynes, *CRC Handbook of Chemistry and Physics, 94th Edition*, 2013.